Scaffold with a Natural Mesh-like Architecture: Isolation, Structural, and in Vitro Characterization

Krishna Burugapalli,[†,‡] Anilkumar Thapasimuttu,[†,‡] Jeffrey C. Y. Chan,[†,‡,§] Li Yao,[†,‡] Sarah Brody,[†,‡] Jack L. Kelly,[§] and Abhay Pandit*[,†,‡]

Department of Mechanical and Biomedical Engineering, National University of Ireland, Galway, Republic of Ireland, National Centre for Biomedical Engineering Science, National University of Ireland, Galway, Republic of Ireland, and Department of Plastic, Reconstructive and Hand Surgery, University College Hospital, Galway, Republic of Ireland

Received November 16, 2006

An intact extracellular matrix (ECM) with a mesh-like architecture has been identified in the peri-muscular subserosal connective tissue (PSCT) of cholecyst (gallbladder). The PSCT layer of cholecyst wall is isolated by mechanical delamination of other layers and decellularized with a treatment with peracetic acid and ethanol solution (PES) in water to obtain the final matrix, which is referred to as cholecyst-derived ECM (CEM). CEM is cross-linked with different concentrations of glutaraldehyde (GA) to demonstrate that the susceptibility of CEM to degradation can be controlled. Quantitative and qualitative macromolecular composition assessments revealed that collagen is the primary structural component of CEM. Elastin is also present. In addition, the ultra-structural studies on CEM reveal the presence of a three-dimensional fibrous mesh-like network structure with similar nanoscale architecture on both mucosal and serosal surfaces. In vitro cell culture studies show that CEM provides a supporting structure for the attachment and proliferation of murine fibroblasts (3T3) and human umbilical vein endothelial cells (HUVEC). CEM is also shown to support the attachment and differentiation of rat adrenal pheochromocytoma cells (PC12).

Introduction

The bioactive nature of intact ECM has been the main reason for its use in regenerative applications.[1,2] The sources for intact ECM explored so far include the dermis of the skin,[3−5] the small intestinal submucosa (SIS),[6−12] the urinary bladder mucosa (UBM) and submucosa (UBS),[13−15] the pericardium,[16−18] the basement membrane and stroma of decellularized liver,[19,20] the decellularized tendon,[21−24] and the amniotic membrane.[25−29] Depending on the location, structure, and function of their source organs, the respective ECM are varied in structure and molecular composition.[30] In an effort to identify an intact ECM with homogeneous structural and compositional properties, the cholecyst was chosen as a source. The current study reports the identification, isolation, decellularization, cross-linking, degradation, structural, and in vitro characterization of porcine cholecyst-derived intact ECM.

The characterization of principal material axis, collagen fiber orientation, and mechanical properties of CEM has been reported earlier.[31] However, the source tissue for intact ECM in the cholecyst wall has not been defined so far. To define the tissue (or layer) of interest, the histological structure of porcine cholecyst wall was investigated in this study. CEM being a xenogenic material, the presence of host cells is a case of immunological concern. A peracetic acid treatment method was hence used to decellularize CEM. Peracetic acid treatment has been reported to disinfect as well as decellularize thin intact ECM matrices, while preserving most of the ECM components.[32] Histological methods were used to check the extent of decellularization.

The use of natural materials for tissue engineering applications has two main concerns: low biomechanical stiffness and rapid biodegradation.[33] CEM has been shown to be a weakly anisotropic matrix that has strength and compliance in the range of physiological stresses and strains.[31] In addition, CEM has also been reported to exhibit a consistent and wider range of collagen fiber orientations, which is thought to increase its suitability as a material for multi-axial loading applications.[31] Rapid biodegradation, the second concern regarding natural materials, is commonly overcome by cross-linking. The degradation behavior of CEM has not been reported to date. In the current study, CEM was cross-linked with different concentrations of glutaraldehyde (GA), primarily to establish the possible range of degradation profiles for CEM. GA was used because it is the most commonly used and efficient cross-linker known for collagenous materials.[34] The degree of cross-linking was characterized using differential scanning calorimetry (DSC) and degradation profiles using collagenase susceptibility assay.

The primary structural framework for ECM is provided by collagen.[30] The presence of elastin adds to the elasticity of ECM.[30] The amount and distribution of collagen and elastin in CEM were evaluated in this study, using quantitative calorimetric assays and qualitative histological staining. Another important parameter for a tissue engineering scaffold is its surface topography. Surface topography has been shown to modulate a cell behavior in diverse cell types.[35,36] The surface topography features of CEM were hence quantified using scanning electron microscopy (SEM).

* To whom correspondence should be addressed. Fax: +353 91 563991. E-mail: abhay.pandit@nuigalway.ie.

† Department of Mechanical and Biomedical Engineering, National University of Ireland.

‡ National Centre for Biomedical Engineering Science, National University of Ireland.

§ University College Hospital.

10.1021/bm061088x CCC: $37.00
Published on Web 02/20/2007

Finally, the in vitro ability of porcine CEM to support the attachment and proliferation of murine 3T3 fibroblasts and HUVEC cell lines and the attachment and differentiation of rat PC12 cell line was tested. SEM and fluorescence microscopy were used to show the morphology of cells on CEM. Alamar-Blue cell metabolic activity assay[37,38] was used to demonstrate the viability and proliferation of 3T3 fibroblasts on CEM.

Experimental Section

All reagents unless otherwise stated were purchased from Sigma Ireland Ltd., Dublin, Ireland. Fresh cholecysts taken from market-weight farm-reared pigs (Sean Duffy Exports Ltd., Gort, Ireland) were transported to the laboratory on ice and processed within 6 h of sacrifice.

Histology of Cholecyst Wall. Cholecyst wall samples for histology were processed using standard histopathology processing and staining protocols. Paraffin sections of 5 μm thickness were cut, stained, and examined under a light microscope (BX51 microscope equipped with DP-70 photography system, Olympus Europe, Hamburg, Germany). Mayer's hematoxylin and eosin (H&E) and Masson's trichrome (MT) stains were used to study the general histological structure of cholecyst wall.

Isolation and Decellularization of CEM. The residual liver tissue attached to the cholecyst was trimmed, and bile was drained through a single transverse incision in the neck of the cholecyst. The neck and fundus were trimmed, and the hollow cylindrical body of the cholecyst wall was flattened into a sheet using a single longitudinal incision. The sheets were rinsed free of bile and soaked in three changes of phosphate buffered saline (pH 7.4) (PBS). The mucosa, lamina propria, and part of muscularis were peeled off as a single unit. The remaining layers of muscularis were removed by mechanical delamination. The serosal mesothelium and its underlying connective tissue were then peeled off. Any residual elements were removed by further mechanical delamination. A yellowish translucent sheet, the isolated PSCT, remained.

The isolated PSCT was rinsed in PBS to remove any adsorbed body fluids. Thereafter, repeated distilled water washings with continuous agitation were used to lyse the remaining resident cells. The xenogenic tissue was disinfected as well as decellularized by treatment with 0.15% peracetic acid in 4.8% ethanol solution (PES) in deionized water under constant stirring for 30 min. The samples were washed in PBS to remove residual peracetic acid and cell debris followed by distilled water to remove the buffer salts. The resulting white colored sheet consisted of an intact ECM, which henceforth will be referred to as CEM.

Stereological volume fraction estimations of cell nuclei were made using the point counting method, with the aid of image analysis software (Image Pro, Media Cybernetics, Berkshire, UK) using a method described earlier.[39] Digital images of histological cross-sections of isolated PSCT and final CEM were acquired at 1000× magnification. A point counting test grid (20 × 20 μm per square) containing 35 grid intersections was superimposed on the digital image. The volume fraction of cell nuclei was calculated as the ratio of intersections falling on nuclei to the total number of intersections of the test system falling on the PSCT/CEM cross-section. The stereological estimations presented are averages of counts taken on five fields of view per section, on three sections per block, and a total of five cholecysts.

Cross-linking of CEM. Freeze-dried sheets of CEM weighing about 0.4 g were immersed in 30 mL of GA solutions at different concentrations from 0.0065% to 0.625% (w/v) in phosphate buffer (pH 7.4) for 4 h at room temperature. The GA cross-linked CEM (GAxCEM) samples were then repeatedly washed with PBS followed by distilled water and freeze-dried (Virtis Advantage Freeze Dryer, Gardiner, NY).

Characterization of Cross-linking. Cross-linking of CEM was determined by measuring the shrink temperature and collagenase degradation. The shrinkage temperature was determined using DSC. Calorimetric measurements were performed using a DSC-60 (Shimadzu Europe Ltd., Duisburg, Germany). CEM and GAxCEM matrices, weighing about 5 ± 2 mg, were immersed in deionized water at 4 °C for 1 h. The wet samples were wiped with filter paper to remove excess water and hermetically sealed in aluminum pans. Heating was maintained at a rate of 5 °C/min in the temperature range 25−110 °C with an empty aluminum pan as the reference probe. Shrinkage temperature (T_s) was determined as the onset value of the occurring endothermic peak. The mean value and standard deviation of three independent measurement runs per matrix type and degree of cross-linking were determined.

Bacterial collagenase Type II from *Clostridium histolyticum* (Sigma: C6885, EC 3.4.24.3), with activity of 277 U mg^{-1}, was used for the enzymatic degradation of CEM and GAxCEM. The enzyme was dissolved in a 0.1 M Tris-HCl buffer (pH 7.4) containing 0.005 M $CaCl_2$ and 0.05 mg mL^{-1} NaN_3. A concentration of 10 U of collagenase per mg of CEM/GAxCEM sample was used. At desired time intervals, the collagenase degradation was arrested by snap freezing. After centrifugation at 4 °C, the remaining pellet was repeatedly washed with distilled water, freeze-dried, and weighed.

Structural Characterization of CEM. Quantitative and qualitative structural protein assessment was done using calorimetric assays and histology, respectively. Collagen content in CEM was quantified using a colorimetric assay by hydroxyproline content estimation as previously reported.[40] Elastin content was also determined using an elastin detection kit (Biocolor Fastin Assay kit, Biocolor Ltd., Newtownabbey, Northern Ireland).[41] For the qualitative protein analysis, histology sections of CEM were stained with MT and Verhoeff's van Geison (VVG) stains, and the distribution of collagen and elastin in the cross-section of CEM was studied.

The surface topography of CEM was investigated using SEM. Samples for SEM were fixed in 3% GA for 24 h followed by dehydration in graded alcohol and chemical drying in hexamethyldisilazane. The dried samples were gold coated (Emitech K-550X Sputter Coater, Emitech Ltd., Ashford, Kent, UK). A low-voltage, high-resolution SEM (S-4700 Hitachi Scientific Instruments, Berkshire, UK) was used to capture photomicrographs of both the mucosal (luminal) and the serosal (abluminal) surfaces of CEM at a magnification of 15 000×. Three stereo pairs were captured from random locations on each surface of each CEM sample ($n = 5$) at 15 000×. Angles of 0° and 5° were used to create virtual three-dimensional images of the surface topography. Elevation height, a three-dimensional feature, was quantified by viewing the stereo pairs under a stereoscope and using the following formula:

$$Z = \frac{P}{2\sin(\alpha/2)}$$

where Z is feature height, α is one-half of the angle of the stereo pair, and P is the parallax (measured with stereoscope). One of the images from each pair was then used to measure pore and fiber diameters on the surface with image analysis software (Image Pro, Media Cybernetics, Berkshire, UK). Because of the nonuniform, non-circular shape of pores on the material surface, pore diameter measurements were taken at the widest part of the pore and in a vertical direction. In all cases, 10 features were measured per photomicrograph or stereo pair, and the location of particular features measured was chosen by superimposing a numbered grid on the photomicrograph and using statistical tables of random numbers.

In Vitro Cell Culture. Three cell types, 3T3 fibroblasts, HUVEC, and PC12 cells, were separately cultured on CEM. GAxCEM cross-linked with 0.625% GA was used as a negative control for these studies. Freeze-dried CEM and GAxCEM samples were cut to disks of 12 mm diameter and placed in the wells of a 24-well plate. Before cell seeding, the samples were sterilized with a 10 min treatment with 0.15% peracetic acid and washed thoroughly with sterile Hank's Balanced Salt Solution (HBSS). For 3T3 fibroblast culture, Dulbecco's Modified Eagle's Medium (DMEM) was supplemented with 10% fetal bovine serum (FBS), 1% (v/v) penicillin−streptomycin (p/s), and 1% L-

glutamine 200 mM. Endothelial cell growth medium-2 (EGM-2) bullet kit (Cambrex Bio Science Wokingham, Ltd., Berkshire, UK) was used for HUVEC cells. In the case of PC12 cells, prior to seeding, the cells were grown overnight in DMEM supplemented with 10% horse serum, 5% FBS, and 1% p/s. The PC12 cells were then suspended in DMEM with 1% horse serum and used for seeding. PC12 cells were seeded both in the presence and in the absence of neuronal growth factor (NGF). NGF treatment was administered by adding 50 ng/mL NGF in 1% serum to the culture medium at the time of cell seeding. For 3T3 and HUVEC cells, the cell seeding density was 50 000 cells per well, while for PC12 it was 30 000 cells per well. The culture media were changed at 1, 3, 5, 6, and 7 days.

The viability and proliferation of 3T3 fibroblasts on CEM were studied by monitoring their metabolic activity using AlamarBlue assay. At 1, 3, and 8 days after seeding, cell-seeded CEM/GAxCEM samples were rinsed with Hank's Balanced Salt Solution (HBSS) and immersed in 500 μL of HBSS containing 10% (v/v) AlamarBlue reagent (Biosource International, CA). After 1 h of incubation, fluorescence was measured, using excitation and emission wavelengths of 528 and 590 nm in microplate fluorescence reader (FLx800, Bio-Tek Instruments, Inc., Vermont). A standard curve was used to extrapolate cell numbers from fluorescence values.

The morphology of the cells on CEM/GAxCEM was studied using SEM and fluorescent staining. At 3 and 6 days after seeding, the cell-seeded and non-cell-seeded control scaffolds were washed with HBSS and processed for SEM using the protocol described above. For fluorescent staining, the scaffolds were fixed in 4% paraformaldehyde for 15 min. The cells were permeabilized with 0.2% Triton X-100 and stained with rhodamine phalloidin (Molecular Probes, Bio Sciences Ltd., Dublin, Ireland) using 1:100 dilution for 1 h at room temperature. The stained cells on scaffolds were examined under light microscope (BX51 inverted microscope equipped with DP-70 photography system, Olympus Europe, Hamburg, Germany). For NGF-treated PC12 cells, the length of the longest neurite of each cell was measured using digital images and image analysis software (Volocity, Improvision Ltd., Coventry, England).

Statistical Analysis. Statistical analysis was performed using statistical software (SPSS 14.0 for windows). Statistical variance between groups was determined by one-way analysis of variance (ANOVA). Tukey's honestly significant difference test was used for post hoc multiple comparisons. A p value of <0.05 was considered to be statistically significant. Data are reported as the mean $\pm$ SD.

Results

Histology of Cholecyst Wall. The histological structure of porcine cholecyst wall is shown in Figure 1. On its luminal surface, the cholecyst wall is lined with a single layer of columnar epithelium (CE). The epithelium rests on a basement membrane (BM), which is continuous with the lamina propria (LP). The epithelial lining, lamina propria, and muscularis mucosae are collectively referred to as "mucosa". The layer muscularis mucosae of mucosa and "submucosa" are absent in cholecyst. Instead, adjacent to lamina propria is "muscularis externa". This layer consists of loosely arranged smooth muscle (SM) bundles, interlaced with collagenous fibers, running in circular, longitudinal, and circumferential directions of the cholecyst wall. External to the muscularis externa is a thick layer of connective tissue (PSCT). The PSCT is mainly composed of ECM and has low cell content. Fibroblasts are the primary resident cells in this layer. Adipocytes and blood vessels are also present and anchored on its abluminal side. On the peritoneal side of the PSCT is "serosa", which consists of thin connective tissue and peritoneal mesothelium. At the cholecyst−liver interface, the PSCT is in direct contact with the liver tissue.

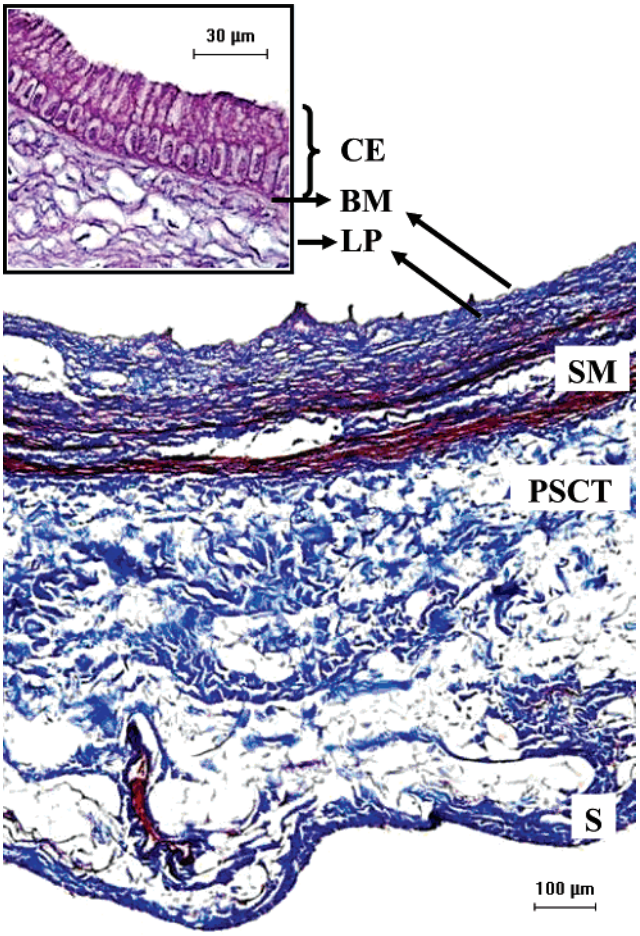

Figure 1. Light micrograph showing the histological appearance of a Masson's trichrome stained cross-section of porcine cholecyst wall; LP, lamina propria; SM, smooth muscle; PSCT, perimuscular subserosal connective tissue; S, serosa. Inset: hematoxylin and eosin stained section showing the columnar epithelium (CE) on basement membrane (BM).

Isolation and Decellularization of CEM. The isolated PSCT layer appears as a semi-transparent yellowish membrane without any remarkable surface features. After decellularization with PES treatment, the CEM samples are white in color. Figure 2a and b shows the histology of the cross-sections of isolated PSCT and final CEM, respectively. The section of PES-treated CEM is devoid of cells. Stereological estimation demonstrated that the cell nuclei account for a volume fraction of 0.97 $\pm$ 0.15% of the isolated PSCT and 0.00 $\pm$ 0.00% for the decellularised CEM ($p < 0.05$).

Characterization of Cross-linking. The shrink temperatures for CEM and GAxCEM matrices are shown in Figure 3. The results indicate differences in the hydrothermal stability of scaffolds depending on the degree of cross-linking. The shrink temperature increased with increasing GA cross-linking. Significant differences were observed between the different samples ($p < 0.05$), except between the CEM samples cross-linked with 0.313% and 0.625% GA ($p = 0.81$).

Figure 4 illustrates the percentage weight remaining of CEM/GAxCEM sample in the presence of collagenase enzyme as a function of time. The rate of weight loss decreased with increasing GA cross-linking. Cross-linking with GA concentration of 0.052% was sufficient for 100% inhibition of degradation of CEM by collagenase enzyme. The weight remaining for non-cross-linked CEM was significantly lower ($p < 0.05$) when compared to all of the GAxCEM samples at all time points,

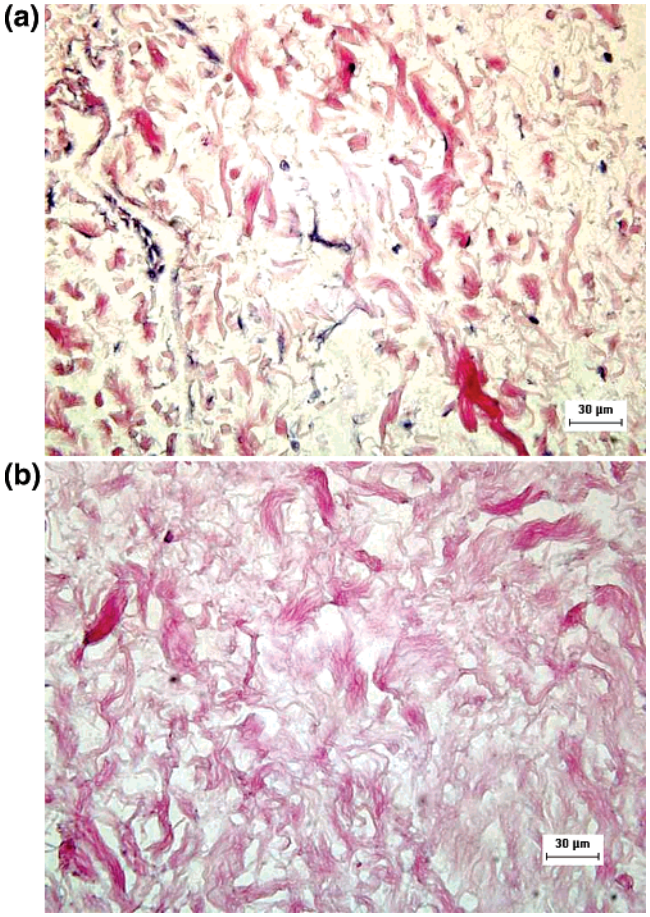

Figure 2. Light micrographs showing the histological appearance of the cross-section of CEM. (a) Non-decellularized and (b) decellularized (hematoxylin and eosin staining).

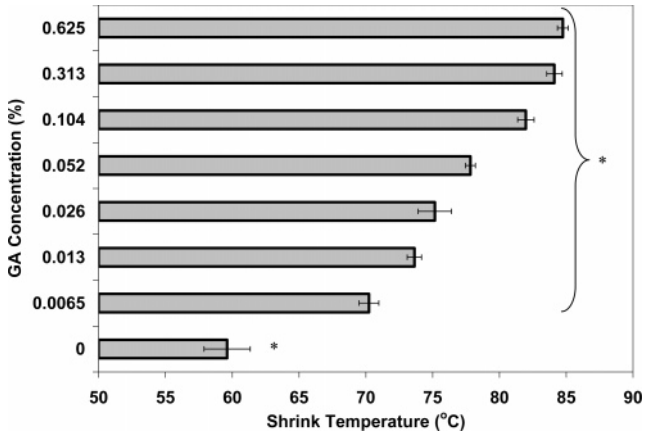

Figure 3. Shrink temperature (T_s) of non-cross-linked and cross-linked CEM matrices as a function of GA cross-linking concentration. T_s is determined as the onset value of the occurring endothermic peak in DSC-calorimetric measurements ($n = 3$). * indicates statistical difference ($p < 0.05$).

with the exception of 0.0065% GAxCEM at 48 h. For GAxCEM samples, no significant differences were observed between samples cross-linked with 0.052% and higher concentrations of GA at all time points. In contrast, for each of the samples cross-linked with 0.0065% and 0.013% of GA, a significant difference was observed ($p < 0.05$) when compared to all other GAxCEM samples at all time points.

Structural Characterization of CEM. Quantitative assessments using hydroxyproline and Biocolor Fastin assays reveal that 75.5 ± 15.1% and 13.3 ± 4.4% of the dry weight of isolated

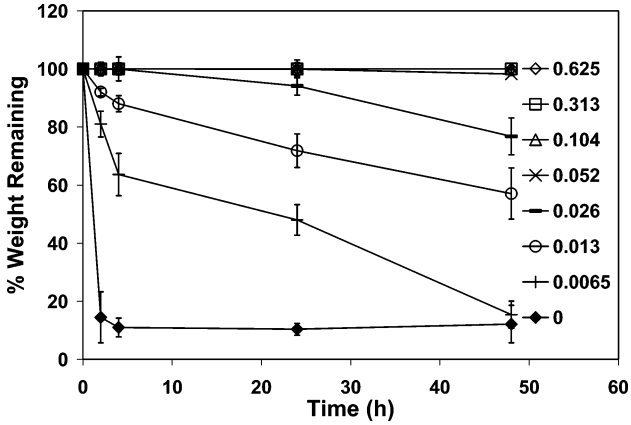

Figure 4. Collagenase degradation of CEM as a function of GA cross-linking ($n = 4$).

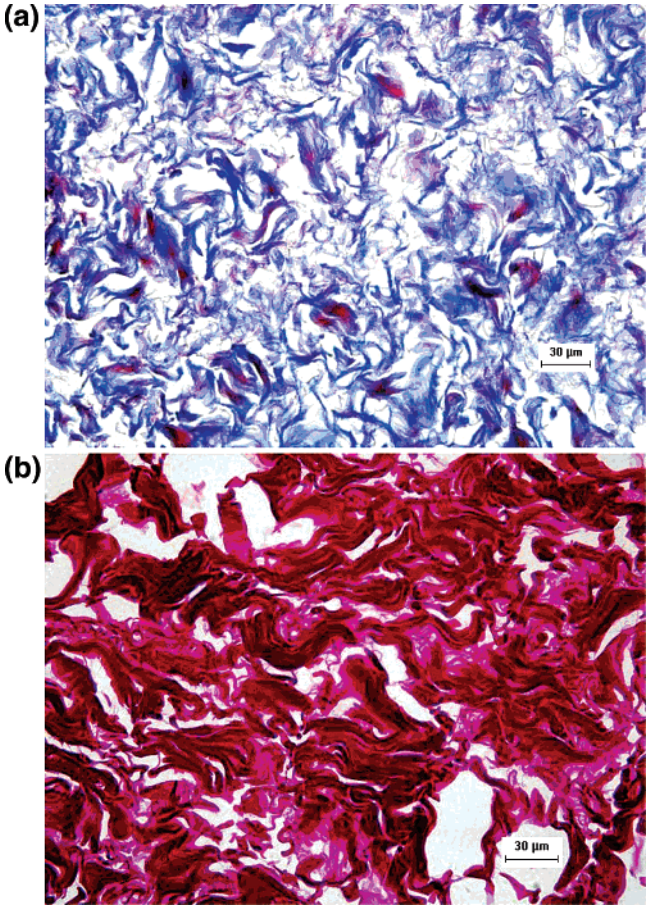

Figure 5. Light micrographs showing the histological appearance of the cross-section of CEM. (a) Masson's trichrome and (b) Verhoeff van Geison.

PSCT is collagen and elastin, respectively. After PES treatment, the CEM is 81.2 ± 6.5% collagen and 7.4 ± 1.0% elastin. No statistical significance was observed between non-decellularized ($n = 4$) and decellularized samples ($n = 4$) for both collagen and elastin assay results.

Qualitative assessments using histology reveal the distribution of collagen and elastin in the cross-section of CEM (Figure 5a and b). Collagen, the primary structural component of CEM, is indicated by the blue staining as illustrated in Figure 5a. The irregularly oriented collagen bundles are uniformly distributed throughout the cross-section of CEM. The black staining in Figure 5b illustrates the distribution of elastin in CEM. Elastin

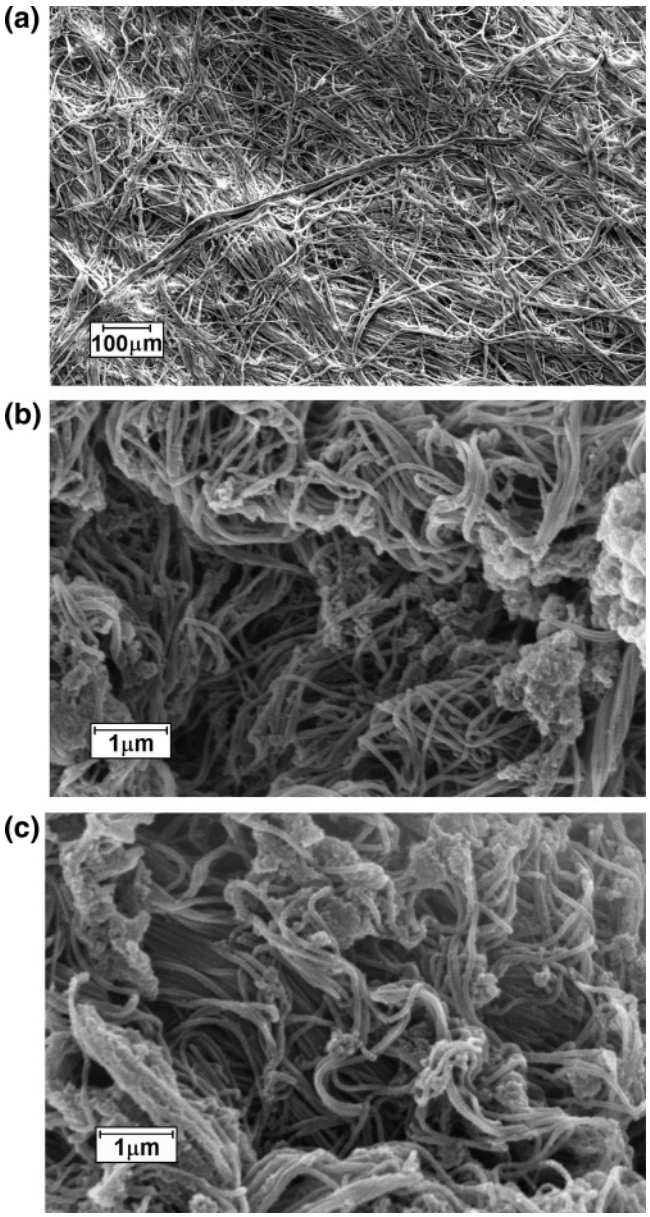

Figure 6. Scanning electron micrographs of CEM showing (a) the mesh-like network structure of CEM and its porous (b) mucosal (luminal side) and (c) serosal (abluminal side) surfaces.

fibers appear to be associated with and running parallel to the longitudinal axis of collagen bundles.

SEM photomicrographs reveal the 3-D fibrous structure of CEM. The fibers are randomly arranged in a loose, mesh-like network (Figure 6a). High-resolution scanning electron micrographs were captured, allowing accurate topographical measurements of the mucosal (Figure 6b) and serosal (Figure 6c) surfaces of the CEM. The mean fiber diameters were 74 ± 4 nm on the mucosal surface and 80 ± 5 nm on the serosal surface, and the mean pore diameters were 216 ± 24 and 264 ± 48 nm, respectively (Table 1). Using a stereological method, mean pore elevation heights were calculated on the mucosal and serosal sides of CEM and were 316 ± 47 and 295 ± 38 nm, respectively (Table 1). No statistical differences in the analyzed feature sizes were observed between those taken on the mucosal and serosal sides of the CEM.

In Vitro Cell Culture. 3T3 fibroblasts were seeded on CEM/GAxCEM scaffolds to determine cell proliferation, morphology, and cell−matrix interactions. The results of the AlamarBlue cell viability and proliferation assay on 3T3 fibroblasts are presented

Table 1. Surface Features Measured through Scanning Electron Microscopy Photomicrographs, Including Stereo Pairs, on Both the Mucosal and the Serosal Surfaces of CEM ($n = 6$, Data Expressed as Mean ± SD)

	mucosal surface	serosal surface
pore diameter		
mean ± SD (nm)	216 ± 24	264 ± 48
range (nm)	13−617	26−846
fiber diameter		
mean ± SD (nm)	74 ± 4	80 ± 5
range (nm)	29−155	37−219
elevation height		
mean ± SD (nm)	316 ± 47	295 ± 38
range (nm)	67−1003	67−902

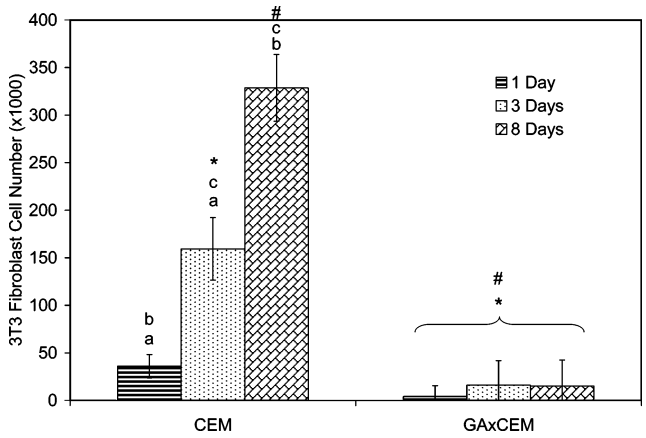

Figure 7. Number of viable cells on 3T3 fibroblast seeded CEM/GAxCEM scaffolds as a function of time, as determined using Alamarblue assay. a, b, c, *, and # indicate significant difference ($p < 0.05$).

in Figure 7. The number of viable cells on CEM increased with time. Significant difference ($p < 0.05$) was observed among the time points 1, 3, and 8 days for the viable cell numbers on CEM. In the case of GAxCEM, the number of viable 3T3 cells was low, and no statistical difference was observed between time points. Significant difference was observed for cells on CEM and GAxCEM at 3 and 8 days.

The phenotype of 3T3 fibroblasts cultured in the free-floating CEM scaffolds differed markedly from the flattened, lamellar appearance characteristic of fibroblasts on planar surfaces on culture plates. Figure 8a and b illustrates the SEM and fluorescence light micrographs of 3T3 fibroblasts on CEM at 6 days. The fibroblasts showed a dendritic phenotype. The main body of the cells was rounded or elongated. Extended from the main body are multiple dendritic processes for attachment with fibers on CEM and neighboring cells (Figure 8a). The three-dimensional dendritic network of extensions of fibroblasts in CEM scaffold can be visualized by phalloidin staining for actin (Figure 8b).

The attachment and proliferation of HUVECs on CEM was also studied to evaluate any possible negative effects due to CEM. Figure 9a and b illustrates the phalloidin staining for actin filaments in HUVECs cultured on the free-floating CEM scaffold at 3 and 6 days, respectively. The endothelial cells were well spread on CEM, and the number of cells increased with time (Figure 9a and b). Furthermore, it was observed that the actin filaments were organized into predominantly dense bands at the cell periphery.

For both 3T3 and HUVECs, at both 3 and 6 day time points, the SEM pictures revealed that the morphology of the surface

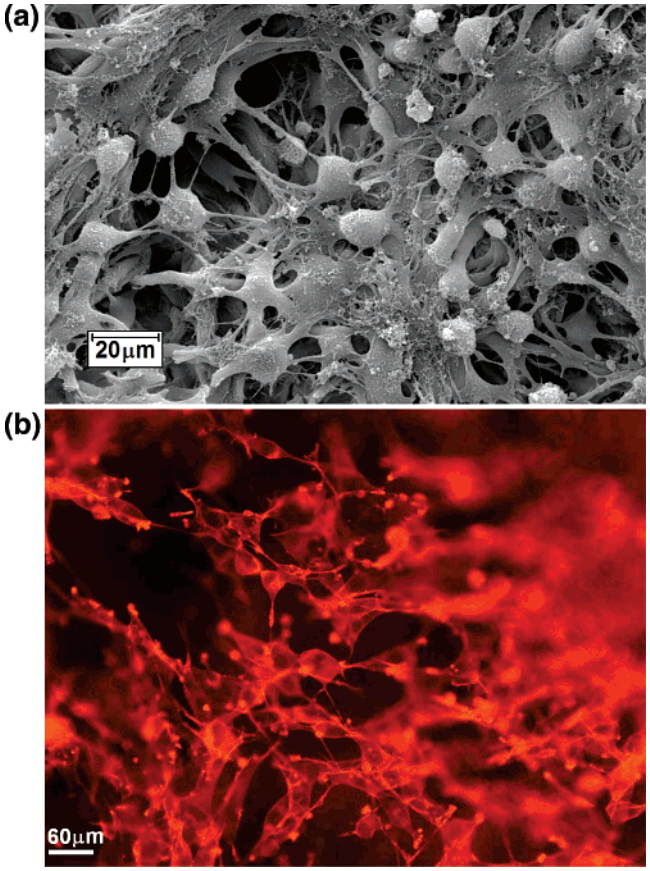

Figure 8. Photomicrographs of 3T3 fibroblasts on CEM at 6 days. (a) SEM and (b) rhodamine phalloidin staining.

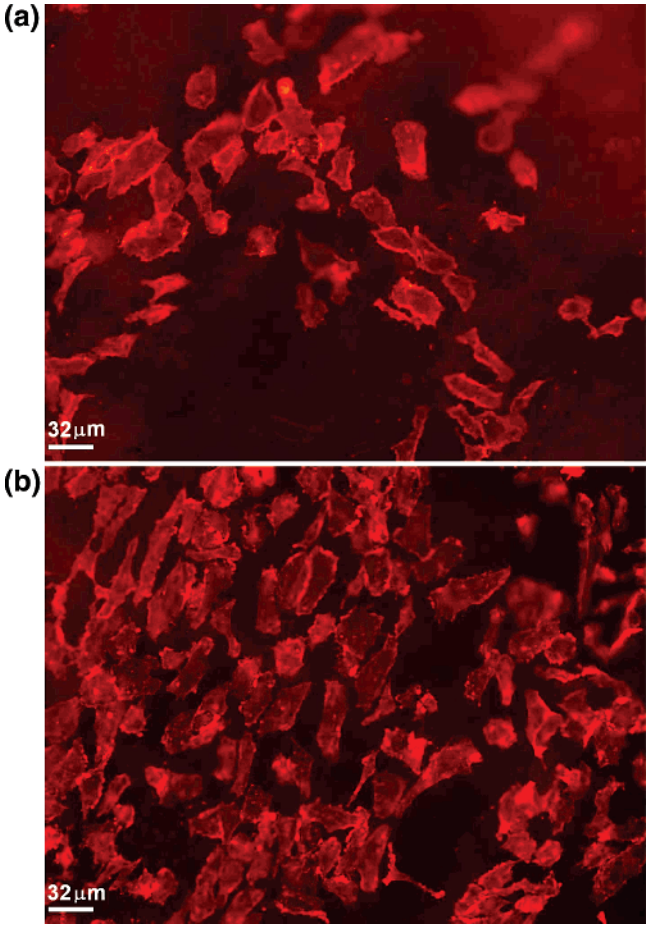

Figure 9. Rhodamine phalloidin stained HUVECs on CEM (a) at 3 days and (b) at 6 days.

of GAxCEM scaffolds seeded with cells was similar to that observed with non-cell-seeded CEM controls. No cell attachment could be detected on the surface of any of the GAxCEM scaffolds seeded with cells.

PC12 cells were cultured on free-floating CEM scaffolds to study the attachment and differentiation behaviors. Figure 10a−c illustrates the attachment and differentiation of PC12 cells on CEM. The undifferentiated PC12 cells were rounded (Figure 10a), while differentiated cells (Figure 10b and c) showed the typical morphology for a neuronal cell. Multiple neurites were observed for the differentiated cells. The length of the longest neurite of each cell was determined on digital images of phalloidin stained cells. The neurite length increased significantly with time from 32.6 ± 2.4 μm at 3 days to 81.7 ± 4.7 μm at 6 days ($p < 0.05$).

Discussion

In the current study, an evaluation of the porcine cholecyst as a potential source for intact ECM was done. The histological structure of porcine cholecyst wall shown in Figure 1 is similar to that reported for human cholecyst.[30,42] Unlike other hollow organs including oesophagus, small intestine, and urinary bladder, cholecyst is a thin-walled organ, whose muscularis layer is composed of loose smooth muscle bundles interlaced with abundant collagenous connective tissue, instead of a well-organized thick smooth muscle tissue. Submucosa, which is commonly used as a source for intact ECM, is absent in cholecyst.[30,42] Instead, the PSCT of cholecyst can be isolated as an intact ECM. The current study reports the isolation and characterization of the PSCT layer of porcine cholecyst as an intact ECM. The porcine cholecyst is a common byproduct of abattoir industry and can be used as a renewable source for intact ECM.

Peracetic acid treatment has been reported to not only decellularize[32] but also disinfect[43,44] thin intact ECM matrices. The PES treatment is the choice for this study because it was demonstrated that most of the bioactive components of ECM are retained in the final matrix.[2] Current study further confirms that a short treatment with PES is sufficient to decellularize the intact ECM derived from cholecyst. Stereological estimations on histology sections demonstrated a 100% disruption of cells with PES treatment (Figure 2a and b). However, no decellularization is 100% efficient in removal of cellular components from isolated xenogenic tissues, and residual DNA can be present in decellularized tissues.[2] The residual amounts of DNA in decellularized CEM are not quantified in this study. The amounts of collagen and elastin in CEM were quantified. The amount of collagen increased, while that of elastin decreased after decellularization. However, no statistical difference was observed for the amounts of both collagen and elastin between the decellularized and non-decellularized CEM samples. The removal of cellular content of the PSCT tissue could result in the relative increase in the amount of insoluble collagen in CEM. The relative reduction in the quantity of elastin in CEM could be due to the extraction of low molecular weight components of elastin by peracetic acid and ethanol.

GA cross-linking of collagenous matrices involves the reaction of free amino groups of lysine or hydroxylysine amino acid residues of the polypeptide chains with the aldehyde groups of GA.[45,46] This reaction is highly efficient in the stabilization

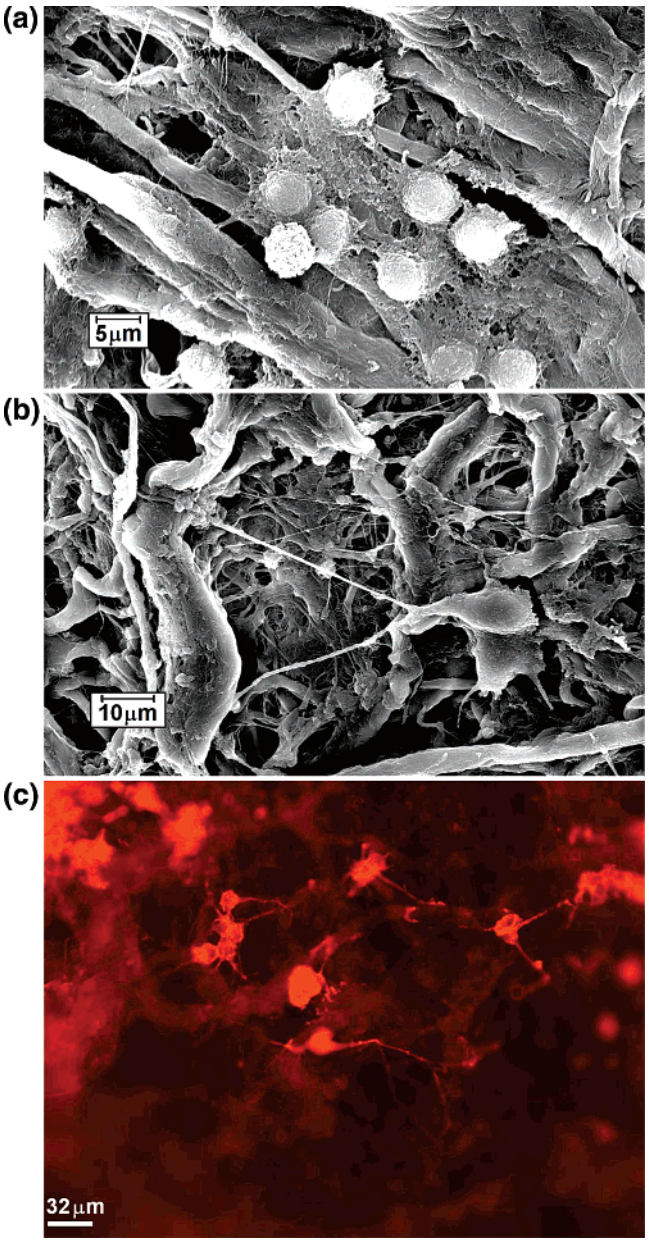

Figure 10. Photomicrographs of PC12 cells at 6 days on CEM (a) in the absence of NGF (SEM), (b) in the presence of NGF (SEM), and (c) in the presence of NGF (rhodamine phalloidin staining).

of collagenous materials. The extent of intra- and intermolecular cross-linking is proportional to the degree of cross-linking, which is reflected in the hydrothermal stability of the cross-linked matrix (Figure 3). CEM has a shrink temperature of 59.6 ± 1.7 °C, which increased to 70.2 ± 0.7 °C when cross-linked with 0.0065% GA, indicating the efficiency of GA cross-linking. The shrink temperature further increased to about 84.1 ± 0.58 °C with a cross-linking concentration of 0.313% GA and plateaus thereafter (no significant difference was observed for shrink temperature between 0.313% and 0.625% GA cross-linking), indicating a maximal cross-linking.

Collagenase digestion assays have been used to evaluate the resistance of collagen-based scaffolds to enzymatic degradation.[47−49] A maximum weight loss of 89% of the dry weight is observed, indicating the high content of collagen in CEM. The susceptibility of CEM to collagenase could be controlled by varying the degree of cross-linking with GA (Figure 4). The influence of GA and other chemical cross-linking treatments on collagenase degradation of collagen-based materials has been previously reported.[48,49] As the degree of cross-linking increases, the ability of enzymes to penetrate the matrix decreases and the introduction of cross-links into the matrix would also mean that more chains have to be cleaved before a degraded fragment can be solubilized.[48,49] The results presented in Figure 4 suggest the degradation profiles possible for CEM.

The amount and distribution of collagen and elastin in the ECM are probably an adaptation to suit the function of the cholecyst. In the absence of a well-organized muscularis externa, the ECM of PSCT could be the principal structural component maintaining the shape and size of the cholecyst. The mesh-like organization (Figure 5) of CEM having a wide and consistent distribution of collagen fiber orientations[31] along with elastin in PSCT could be responsible for the strength of the cholecyst wall. The adequate strength and stiffness of isolated CEM reported by Coburn et al.[31] support this hypothesis. In situ, this loosely organized ECM anchors the smooth muscle layer on the mucosal side and blood vessels and adipose tissue on the serosal side. When these layers are removed to obtain the CEM, both mucosal and serosal surfaces have similar macroscopic appearance. The fibrous network on both surfaces is less densely organized. In this respect, CEM is different from ECM derived from submucosa of small intestinal and urinary bladder, which have a dense mucosal surface and a less densely organized serosal surface.[50]

CEM topography resembles that of previously studied anatomical layers, which facilitate the growth of cells in vivo.[35,36] Quantification of surface topography features for CEM revealed no statistically significant difference in the measured features between the mucosal and serosal surfaces (Table 1). All surface features (mean fiber diameter, mean pore diameter, and pore elevation) are in the nanoscale range, and high standard deviations indicate roughness of both CEM surfaces. Nanoscale biological length topographic features have been shown to strongly modulate a variety of fundamental cell behaviors in diverse cell types.[51−53] For instance, recent studies on the response of epithelial cells to a ridge-and-groove-type substratum with pitches ranging from 400 to 4000 nm indicated that at a pitch of 400 nm cells are aligned and elongated with the ridges, while at a pitch of 4000 nm the effects of topography are lost.[53] Therefore, the incorporation of biologic length scale features is a critical parameter in characterizing a biomaterial for regenerative applications. CEM demonstrates a wide range of surface pore sizes ranging between 13 and 846 nm, averaging between 200 and 300 nm (Table 1). This wide range of pore sizes, in addition to the bioactive nature of the intact ECM, can facilitate the attachment and migration of a variety of cells essential in vivo.

ECM has been shown to contain receptors and other bioactive agents that aid in cell attachment, migration, proliferation, and differentiation and in regulatory functions.[54−59] The results of the current study, discussed below, suggest that the intact ECM derived from the porcine cholecyst, CEM, has the ability not only to support the attachment and proliferation of different cells but also to promote differentiation on providing the right stimulus.

3T3 fibroblasts attached and proliferated on CEM. The 3T3 fibroblasts proliferated to near confluence on CEM by 6 days of culture (Figure 7). The fibroblasts cultured on CEM developed an in-situ-like morphology as compared to cells on planar surfaces. A similar phenotype has been reported for fibroblasts grown on collagen matrices.[60] The dendritic extensions of the fibroblasts cross-linked the fibers of CEM to form a three-dimensional network (Figure 8a and b). Cross-linking

behavior has also been reported for fibroblasts cultured on synthetic biodegradable electrospun membranes.[61] Furthermore, the dendritic extensions of the fibroblasts on CEM also contained actin filaments concentrated at their tips (Figure 8b). Such concentration of actin filaments could also indicate a role in focal adhesion with surrounding fibers and cells.[60] Interconnections between cells on CEM can also be visualized in Figure 8a. These connections between cells may have a role in homeostatic regulation through metabolic coupling similar to that reported for fibroblasts on collagen matrices.[60]

Glutaraldehyde cross-linking has been shown to cause cell death in vitro.[62] At both 3 and 6 day time points, the topography of cell seeded GAxCEM was similar to that of non-seed control CEM. Even after thorough washings, GAxCEM samples failed to support cell attachment and proliferation (Figure 7). The failure of cell attachment on GAxCEM can be attributed to the residual toxicity of GA. Capping of the aldehyde residues of GA could reduce its toxicity.[62] Alternatively, less toxic methods such as carbodiimide[63] and transglutaminase[37,64] cross-linking methods can be used, if a prolonged in vivo shelf life is desired.

Human endothelial cells have often been used for in vitro cytotoxicity testing.[65] In this study, HUVECs were primarily used to test any cytotoxicity due to CEM. No apparent cytotoxicity was observed. The cell numbers increased with time, indicating proliferation of HUVECs on CEM (Figure 9a and b). In addition, the HUVECs showed a well-spread morphology, with actin filaments predominantly organized as dense bands at the cell periphery (Figure 9a and b). These aggregations could be focal adhesion sites[66] for binding with fibers of CEM.

PC12 cells have often been used as a prototype for neurogenic study, because they display behavior similar to that of differentiated sympathetic neurons upon exposure to neuronal growth factor (NGF). Introduction of bioactive agents such as fibronectin[67] and laminin[68] onto biomaterials has been shown to modulate the differentiation of PC12 cells. PC12 cells were cultured on CEM to study the attachment and differentiation behaviors. PC12 cells attached (Figure 10a) and differentiated (Figure 10b and c) upon stimulation with NGF on CEM. In the absence of NGF, the PC12 cells had a rounded morphology (Figure 10a). Addition of NGF to the culture medium resulted in the development of multiple neuritis on the PC12 cells, and the length of the neurites increased with time. This result clearly indicated the ability of PC12 cells to differentiate on CEM.

In summary, a new source for an intact ECM was identified in the PSCT layer of the porcine cholecyst wall. The PSCT layer was isolated by mechanical delamination of other layers of cholecyst wall and decellularized with a treatment with a solution of peracetic acid and ethanol in water. The resulting thin membrane-like scaffold, which is referred to as CEM, had a mesh-like architecture. CEM is a preformed substrate, which in its native form (without cross-linking) is stronger, pliable, slower degrading, and faster and more economical to prepare as compared to purified ECM substrates such as collagen matrices. As compared to similar substrates such as SIS, UBM, and UBS, CEM has been shown to be stronger in an earlier study.[31] Furthermore, CEM has also been shown to have a wider and consistent orientation of collagen fibers in its matrix, as compared to the higher degree of orientation for SIS.[31] The better mechanical properties can be attributed to the presence of elastin, as determined in the current study, and the wide range of collagen orientations observed in an earlier study.[31] The current study also demonstrated the controllability of degradation of CEM. In addition, CEM had a similar nanoscale roughness on both its mucosal side and its serosal side surfaces, which is conducive for cell attachment, migration, and differentiation. 3T3 fibroblasts differentiated on CEM to a phenotype similar to that observed in situ. Cells on CEM showed behavior similar to that observed on collagen matrices. No apparent cytotoxicity to HUVECs could be observed due to CEM. CEM, in its native non-cross-linked form, supported the differentiation of PC12 cells. Considering its adequate mechanical properties,[31] controllable degradation, mesh-like architecture, nanoscale topography, and ability to support the attachment and proliferation of a variety of cells, CEM is a promising candidate biomaterial for a variety of tissue engineering applications including peripheral nerve regeneration.

Acknowledgment. K.B. and A.T. contributed equally to this work. We thank Enterprise Ireland, European FP6-Marie Curie TOK Award, and the Irish Council for Science, Engineering, and Technology (IRCSET), which is funded under the National Development Plan, for supporting this research.

References and Notes

(1) Hodde, J. *Tissue Eng.* **2002**, *8*, 295−308.
(2) Badylak, S. F. *Semin. Cell Dev. Biol.* **2002**, *13*, 377−383.
(3) Wainwright, D. J. *Burns* **1995**, *21*, 243−248.
(4) Inoue, Y.; Anthony, J. P.; Lleon, P.; Young, D. M. *J. Reconstr. Microsurg.* **1996**, *12*, 307−311.
(5) Costantino, P. D.; Wolpoe, M. E.; Govindaraj, S.; Chaplin, J. M.; Sen, C.; Cohen, M.; Gnoy, A. *Head Neck* **2000**, *22*, 765−771.
(6) Badylak, S. F.; Lantz, G. C.; Coffey, A. C.; Geddes, L. A. *J. Surg. Res.* **1989**, *47*, 74−80.
(7) Kropp, B. P.; Badylak, S. F.; Thor, K. B. In *Muscle, Matrix, and Bladder Function*; Zedric, S., Ed.; Plenum Press: New York, 1995; pp 229−235.
(8) Matheny, R. G.; Hutchison, M. L.; Dryden, P. E.; Hiles, M. D.; Shaar, C. J. *J. Heart Valve Dis.* **2000**, *9*, 769−774.
(9) Badylak, S.; Kokini, K.; Tullius, B.; Whitson, B. *J. Surg. Res.* **2001**, *99*, 282−287.
(10) Prevel, C. D.; Eppley, B. L.; Summerlin, D. J.; Sidner, R.; Jackson, J. R.; McCarty, M.; Badylak, S. F. *Ann. Plast. Surg.* **1995**, *35*, 381−388.
(11) Cobb, M. A.; Badylak, S. F.; Janas, W.; Simmons-Byrd, A.; Boop, F. A. *Surg. Neurol.* **1999**, *51*, 99−104.
(12) Hodde, J. P.; Badylak, S. F.; Shelbourne, K. D. *Tissue Eng.* **1997**, *3*, 27−37.
(13) Kanematsu, A.; Yamamoto, S.; Noguchi, T.; Ozeki, M.; Tabata, Y.; Ogawa, O. *J. Urol.* **2003**, *170*, 1633−1638.
(14) Wefer, J.; Sievert, K. D.; Schlote, N.; Wefer, A. E.; Nunes, L.; Dahiya, R.; Curtis, G. A.; Tanagho, E. *J. Urol.* **2001**, *165*, 1755−1759.
(15) Merguerian, P. A.; Reddy, P. P.; Barrieras, D. J.; Wilson, G. J.; Woodhouse, K.; Bagli, D. J.; McLorie, G. A.; Khoury, A. E. *Br. J. Urol.* **2000**, *85*, 894−898.
(16) Goncalves, A. C.; Griffiths, L. G.; Anthony, R. V.; Orton, E. C. *J. Heart. Valve Dis.* **2005**, *14*, 212−217.
(17) Kambic, H.; Kay, R.; Chen, J. F.; Matsushita, M.; Harasaki, H.; Zilber, S. *J. Urol.* **1992**, *148*, 539−543.
(18) Yen, C.; Huang-Chien, L.; Hao-Ji, W.; Chih-Ping, C.; Hsing-Wen, S. *J. Biomed. Mater. Res.* **2004**, *69A*, 323−333.
(19) Lin, P.; Chan, W. C. W.; Badylak, S. F.; Bhatia, S. N. *Tissue Eng.* **2004**, *10*, 1046−1053.
(20) Burra, P.; Tomat, S.; Conconi, M. T.; Macchi, C.; Russo, F. P.; Parnigotto, P. P.; Naccarato, R.; Nussdorfer, G. G. *Int. J. Mol. Med.* **2004**, *14*, 511−515.
(21) Ramesh, R.; Kumar, N.; Sharma, A. K.; Maiti, S. K.; Kumar, S.; Charan, K. *J. Vet. Med., Ser. A* **2003**, *50*, 520−526.
(22) Burres, S. *Facial Plast. Surg.* **2004**, *20*, 149−152.
(23) Curtis, R. J.; Delee, J. C.; Drez, D. J. *Am. J. Sports Med.* **1985**, *13*, 408−414.
(24) Thammavaram, K. V.; Benzel, E. C.; Kesterson, L. *South Med. J.* **1990**, *83*, 634−636.
(25) De Rotth, A. *Arch. Ophthalmol.* **1940**, *23*, 522−525.
(26) Robson, M. C.; Krizek, T. J.; Koss, N.; Samburg, J. L. *Surg. Gynecol. Obstet.* **1973**, *136*, 904−906.
(27) Kim, J. C.; Tseng, S. C. *Cornea* **1995**, *14*, 473−484.

(28) Szabo, A.; Haj, M.; Waxsman, I.; Eitan, A. *Eur. Surg. Res.* **2000**, *32*, 125−128.
(29) Mohammad, J.; Shenaq, J.; Rabinovsky, E.; Shenaq, S. *Plast. Reconstr. Surg.* **2000**, *105*, 660−666.
(30) Ross, M. H.; Romrell, L. J.; Kaye, G. I. *Histology, A text book and atlas*, 3rd ed.; Williams & Wilkins: Maryland, 1995; pp 94−104, 507−510.
(31) Coburn, J. C.; Brody, S.; Billiar, K. L.; Pandit, A. *J. Biomed. Mater. Res.*, published online January 31, 2007.
(32) Gilbert, T. W.; Sellary, T. L.; Badylak, S. F. *Biomaterials* **2006**, *27*, 3675−3683.
(33) Koide, M.; Osaki, K.; Konishi, J.; Oyamada, K.; Katakura, T.; Takanashi, A.; Yoshizato, K. *J. Biomed. Mater. Res.* **1993**, *27*, 79−87.
(34) Bigi, A.; Cojazzi, G.; Panzavolta, S.; Rubini, K.; Roveri, N. *Biomaterials* **2001**, *22*, 763−768.
(35) Brody, S.; Anilkumar, T.; Lilensiek, S.; Last, J. A.; Murphy, C. J.; Pandit, A. *Tissue Eng.* **2006**, *12*, 413−421.
(36) Abrams, G. A.; Schaus, S. S.; Goodman, S. L.; Nealey, P. F.; Murphy, C. J. *Cornea* **2000**, *19*, 57−64.
(37) O'Halloran, D. M.; Collighan, R. J.; Griffin, M.; Pandit, A. S. *Tissue Eng.* **2006**, *12*, 1467−1474.
(38) Voytik-Harbin, S. L.; Brightman, A. O.; Waisner, B.; Lamar, C. H.; Badylak, S. F. *In Vitro Cell Dev. Biol. Anim.* **1998**, *34*, 239−46.
(39) Garcia, Y.; Breen, A.; Burugapalli, K.; Dockery, P.; Pandit, A. *Biomaterials* **2007**, *28*, 175−186.
(40) Reddy, G. K.; Enwemeka, C. S. *Clin. Biochem.* **1996**, *29*, 225−229.
(41) Fastin Elastin Assay. Biocolor Ltd., 4th ed., 2002; http://www.biocolor.co.uk/manuals/Fastinmanual.pdf.
(42) Frierson, H. F. *Am. J. Surg. Pathol.* **1989**, *13*, 146−162.
(43) Pruss, A.; Kao, M.; Keisewetter, H.; von Vesen, R.; Pauli, G. *Biologicals* **1999**, *27*, 195−201.
(44) Hodde, J.; Hiles, M. *Biotechnol. Bioeng.* **2002**, *79*, 211−216.
(45) Olde Damink, L. H. H.; Dijkstra, P. J.; van Luyn, M. J. A.; van Wachem, P. B.; Nieuwenhuis, P.; Feijen, J. *J Mater. Sci.* **1995**, *6*, 460−472.
(46) Khor, E. *Biomaterials* **1997**, *18*, 95−105.
(47) Zhong, S.; Teo, W. E.; Zhu, X.; Beuerman, R.; Ramakrishna, S.; Yung, L. Y. L. *Biomacromolecules* **2005**, *6*, 2998−3004.
(48) Olde Damink, L. H. H.; Dijkstra, P. J.; van Luyn, M. J. A.; van Wachem, P. B.; Nieuwenhuis, P.; Feijen, J. *Biomaterials* **1996**, *17*, 679−684.
(49) Olde Damink, L. H. H.; Dijkstra, P. J.; van Luyn, M. J. A.; van Wachem, P. B.; Nieuwenhuis, P.; Feijen, J. *J. Biomed. Mater. Res.* **1995**, *29*, 139−149.
(50) Hodde, J. P.; Tullius, R. S.; Badylak, S. F. *Tissue Eng.* **2002**, *8*, 225−234.
(51) Teixeira, A. I.; Abrams, G. A.; Bertics, P. J.; Murphy, C. J.; Nealey, P. F. *J. Cell Sci.* **2003**, *116*, 1881−1892.
(52) Flemming, R. G.; Murphy, C. J.; Abrams, G. A.; Goodman, S. L.; Nealey, P. F. *Biomaterials* **1999**, *20*, 573−588.
(53) Karuri, N. W.; Liliensiek, S.; Teixeira, A. I.; Abrams, G.; Campbell, S.; Nealey, P. F.; Murphy, C. J. *J. Cell Sci.* **2004**, *117*, 3153−3164.
(54) Shin, H.; Jo, S.; Mikos, A. G. *Biomaterials* **2003**, *24*, 4353−4364.
(55) Cukierman, E.; Pankov, R.; Yamada, K. M. *Curr. Opin. Cell Biol.* **2002**, *14*, 633−639.
(56) Schwartz, M. A. *Trends Cell Biol.* **2001**, *11*, 466−470.
(57) Geiger, B.; Bershadsky, A.; Pankov, R.; Yamada, K. M. *Nat. Rev. Mol. Cell Biol.* **2001**, *2*, 793−805.
(58) Hynes, R. O. *Trends Cell Biol.* **1997**, *9*, M33−M77.
(59) Friedl, P. *Curr. Opin. Cell Biol.* **2004**, *16*, 14−23.
(60) Grinnell, F.; Ho, C.; Tamarix, E.; Lee, D. J.; Skuta, G. *Mol. Biol. Cell* **2003**, *14*, 384−395.
(61) Bhattarai, S. R.; Bhattarai, N.; Yi, H. K.; Hwang, P. H.; Cha, D. I.; Kim, H. Y. *Biomaterials* **2004**, *25*, 2595−2602.
(62) Grabenwoger, M.; Sider, J.; Fitzal, F.; Zelenka, C.; Windberger, U.; Grimm, M.; Moritz, A.; Bock, P.; Wolner, E. *Ann. Thorac. Surg.* **1996**, *62*, 772−777.
(63) Angele, P.; Abke, J.; Kujat, R.; Faltermeier, H.; Schumann, D.; Nerlich, B.; Kinner, B.; Englert, C.; Ruszczak, Z.; Mehrl, R.; Mueller, R. *Biomaterials* **2004**, *25*, 2831−2841.
(64) Boderik, E. P.; O'Halloran, D. M.; Rochev, Y. A.; Griffin, M.; Collighan, R. J.; Pandit, A. S. *J. Biomed. Mater. Res.* **2005**, *72B*, 37−42.
(65) Kirkpatrick, C. J.; Otto, M.; van Kooten, T.; Krump, V.; Kriegsmann, J.; Bittinger, F. *J. Mater. Sci.: Mater. Med.* **1999**, *10*, 589−594.
(66) Voskerician, G.; Anderson, J. M.; Ziats, N. P. *J. Biomed. Mater. Res.* **2000**, *51*, 1−9.
(67) Cheng, M.; Deng, J.; Yang, F.; Gong, Y.; Zhao, N.; Zhang, X. *Biomaterials* **2003**, *24*, 2871−2880.
(68) Li, B.; Ma, Y.; Wang, S.; Moran, P. M. *Biomaterials* **2005**, *26*, 1487−1495.

BM061088X